EARTHQUAKE ENGINEERING AND STRUCTURAL DYNAMICS
Earthquake Engng Struct. Dyn. 2012; **41**:987–1000
Published online 21 September 2011 in Wiley Online Library (wileyonlinelibrary.com). DOI: 10.1002/eqe.1170

Shaking table test of the effects of multi-unit particle dampers attached to an MDOF system under earthquake excitation

Zheng Lu[1], Xilin Lu[1,*,†], Wensheng Lu[1] and Sami F. Masri[2]

[1]*State Key Laboratory of Disaster Reduction in Civil Engineering, Tongji University, Shanghai 200092, China*
[2]*Viterbi School of Engineering, University of Southern California, Los Angeles, CA 90089, USA*

SUMMARY

This paper presents the results of an experimental and analytical/computational study of the performance of multi-unit particle dampers with an MDOF system. A series of shaking table tests of a three-storey steel frame with the particle damper system were carried out to evaluate the performance of the system and to verify the analysis method. An analytical solution based on the discrete element method is also presented. A comparison between the experimental and computational results shows that reasonably accurate estimates of the response of a primary system under earthquake excitations can be obtained. These results also indicate that the excitation characterization influences the performance of the particle damper system, for example, particle dampers have good performance in reducing the seismic response of structures and particle movements of plug flow pattern can yield good vibration attenuation effects. It is shown that by using properly designed multi-unit particle dampers, a lightly damped primary system can achieve a reasonable reduction in its response, with a small weight penalty. Copyright © 2011 John Wiley & Sons, Ltd.

Received 10 November 2010; Revised 28 April 2011; Accepted 3 August 2011

KEY WORDS: analytical model; discrete element method; impact; particle damper; passive vibration control; shaking table test

NOMENCLATURE

c_2	damping constant of impact damper 'stops'
c_3	damping constant of the damper between two particles
$\mathbf{F_{ij}^n}$	normal contact force between particle i and particle j
$\mathbf{F_{ij}^t}$	tangential contact force between particle i and particle j
$\mathbf{I_i}$	moment of inertia of particle i
k_2	stiffness of the impact damper "stops"
k_3	stiffness of the spring between two particles
k_i	number of contact particles that are in contact with particle i
$\mathbf{n_{ij}}$	unit vector from the center of particle i to the center of particle j
N	total number of the particles
$\mathbf{p_i}$	position vector of the center of gravity of particle i
$\mathbf{T_{ij}}$	torque between particle i and particle j
μ	mass ratio, which is the ratio of the total mass of particles and the total mass of the primary system
μ_s	coefficient of friction

*Correspondence to: Xilin Lu, State Key Laboratory of Disaster Reduction in Civil Engineering, Tongji University, Shanghai 200092, China.
†E-mail: lxlst@tongji.edu.cn

δ_n normal relative displacement
$\dot{\delta}_n$ normal relative velocity
$\dot{\delta}_t$ tangential relative velocity
Δt_i critical time step
Δ_i distance from the center of particle i to the wall
φ_i angular displacement vector of particle i
ζ_2 damping ratio of impact damper 'stops'
ζ_3 damping ratio of the damper between two particles
ω_2 natural frequency of the impact damper 'stops'
ω_3 natural frequency of the spring between two particles

1. INTRODUCTION

1.1. Background

Structural control plays a very important role in engineering and can be divided into three categories, namely, passive, active, and hybrid control techniques, in which the passive strategy is most widely applied because of its simplicity and lack of power requirements. Among numerous passive devices for structural control applications (e.g., [1–3]), a class of highly nonlinear dampers (particle dampers) that simultaneously utilize momentum transfer and internal energy dissipation offer some advantages in practical situations. Naeim [4] introduced the performance of a tall building with a particle damper system in Santiago, Chile during the 2010 offshore Maule, Chile earthquake. The system performed very well during the earthquake and the building did not suffer any damages above the ground or at any subterranean floors and basement walls.

Impact dampers [5], with their advantages of ruggedness, reliability, and insensitivity to extreme temperatures, are simple and efficient passive devices that are used to attenuate the vibrations of lightly damped structures, through the impact between a solid particle and the primary system to which they are attached. However, during the impact process, impulsive loads are transmitted between the two coupled systems and will cause a high level of noise. Simultaneously, large contact forces will result in material deterioration and local deformation accompanying plastic collisions. To reduce these problems, smaller-sized particles are used to replace the single solid particle, thus resulting in a particle damper. On the other hand, the damping efficiency of particle dampers depends on the container dimensions [6]. When the optimum dimensions of the container are large, the container cannot be attached from a practical design point of view (e.g., there is not enough space because of architectural considerations). In such a case, the damper performance is retained when particle dampers are replaced by multi-unit particle dampers, with a moderate number of small containers.

Many experimental studies and numerical simulations have been carried out for the characterization of particle dampers. Thomas *et al.* [7] tested an impact damper used to improve the chatter performance of a cantilever boring bar. Ema and Marui [8] carried out a fundamental experimental study on impact dampers and achieved the optimum damping effect by adjusting the mass ratio and clearance. Yang *et al.* [9] developed a pair of two-dimensional master design curves with unitless axes that are comprised of combinations of design parameters. Li and Darby [10] conducted a series of investigations to find out the effect of an impact damper on an MDOF system. As to numerical simulations, Papalou and Masri [11–13] introduced an equivalent single-particle impact damper model to evaluate the performance of multiparticle dampers. Liu *et al.* [14] used an equivalent viscous damping model to represent the nonlinearity that was extracted from experimental results. Xu *et al.* [15] presented an empirical method for particle damping design. Fang and Tang [16] developed an improved analytical model by multiphase flow theory based on the previous work of Wu *et al.* [17]. Although these equivalent models or empirical-based studies have given many new insights, they are essentially phenomenological, and the results are difficult to extrapolate beyond their respective experimental conditions. Recently, the discrete element method (DEM) [25], which can take interactions between particles into account, has been used to perform limited studies of particle dampers [18–21].

DOI: 10.1002/eqe

Despite these numerous analytical and experimental studies that have been conducted over the years into the various aspects of the motion of particle dampers, the understanding of the complex particle damping mechanism has still not been well developed because of the system's high nonlinearity and the complexity involving interactions among a large number of parameters under arbitrary dynamic excitations. It can be seen that most of the studies listed above have investigated the interaction between a particle damper (or an impact damper) and an SDOF primary structure. Moreover, most analytical results have focused on single-unit single-particle dampers, multi-unit single-particle dampers, or single-unit multiparticle dampers (shown in Figure 1). Also, many parameters influence the behavior of particle dampers; however, it is not feasible to investigate the numerous particle damper design parameters experimentally. Additionally, shaking table tests of particle dampers attached to a large scale MDOF primary system are seldom investigated in the literature. Consequently, there is a need to carry out a shaking table test of multi-unit multiparticle dampers (henceforth referred to as 'multi-unit particle dampers') when operating with an MDOF system that is subjected to earthquake waves, and to construct an analytical model for calculating the performance of multi-unit particle dampers.

1.2. Scope

This paper first introduces shaking table test results for a three-storey steel frame with a multi-unit particle damper system, then presents an analytical/computational solution based on the DEM to analyze the performance of such a system. Finally, the computational method is programmed, validated, and implemented.

2. EXPERIMENTAL SETUP AND PROCEDURE

The experimental model consisted of a three-storey steel frame as the primary structure and a multi-unit particle damper that was mounted on the top floor. Figure 2 shows the configuration of the model. Additional masses were applied to each floor by bolting them to the floor beam to make the fundamental frequency of the testing frame equal to around 1.0 Hz, which is close to the frequency of a typical high-rise building. The total masses from the first floor to the roof, including the frame self-weight during testing, were 1915 kg, 1915 kg, and 2124 kg, respectively. The primary system had a damping ratio of 0.013. The natural frequencies of the primary system were $f_1 = 1.07$ Hz, $f_2 = 3.2$ Hz, and $f_3 = 4.8$ Hz.

The multi-unit particle dampers were made of steel plates consisting of four rectangular containers with the length × width × height dimensions of 0.49 m × 0.49 m × 0.5 m. They were attached symmetrically with respect to the shaking direction. Learning from the experience of Saeki [18], who did an experiment on a particle damper under harmonic excitation with a 6-mm-diameter steel ball and found that when the cavity length was around 60 mm, the vibration attenuation effect was the best; the diameter of the steel ball bearing was chosen to be 50.8 mm, which was also similar in size to the one used in the tall building Naeim *et al*. [4] introduced. Considering that in real engineering projects, the mass ratio between the damper and the primary structure should be small, a total of 63 steel ball bearings were put into each container, with the total mass of 135 kg, which was

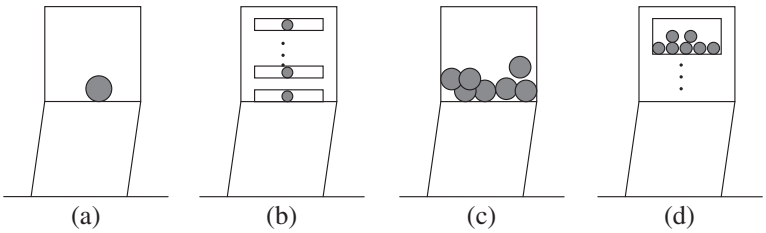

Figure 1. Schematic diagram of various particle damper configurations. (a) Single-unit single-particle damper; (b) Multi-unit single-particle damper; (c) Single-unit multiparticle damper; and (d) Multi-unit multiparticle damper.

DOI: 10.1002/eqe

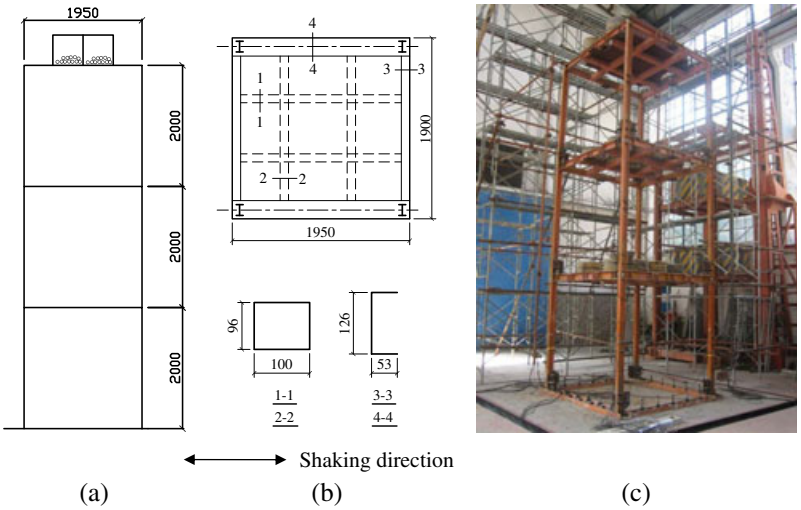

Figure 2. Configuration of frame model with multi-unit particle dampers (unit: mm). (a) Elevation; (b) floor plan; and (c) photo of the experimental model.

2.25% of the primary system mass. The design procedure combined the realistic consideration and the preliminary optimization idea.

Four earthquake time histories of acceleration were selected as the input data during the shaking table test to evaluate the performance of the multi-unit particle damper system under different seismic actions. The four time histories of acceleration were Kobe (1995, NS), El Centro (1940, NS), Wenchuan (2008, NS) (shown in Figure 3), and Shanghai design code specified artificial earthquake accelerogram (SHW2, 1996). All the earthquake time histories of acceleration were inputted in only one direction of the test model and the time interval was 0.02 s. The peak value of the acceleration was increased gradually from 0.05 g to 0.2 g (g is the acceleration due to gravity). The motion of the structure and

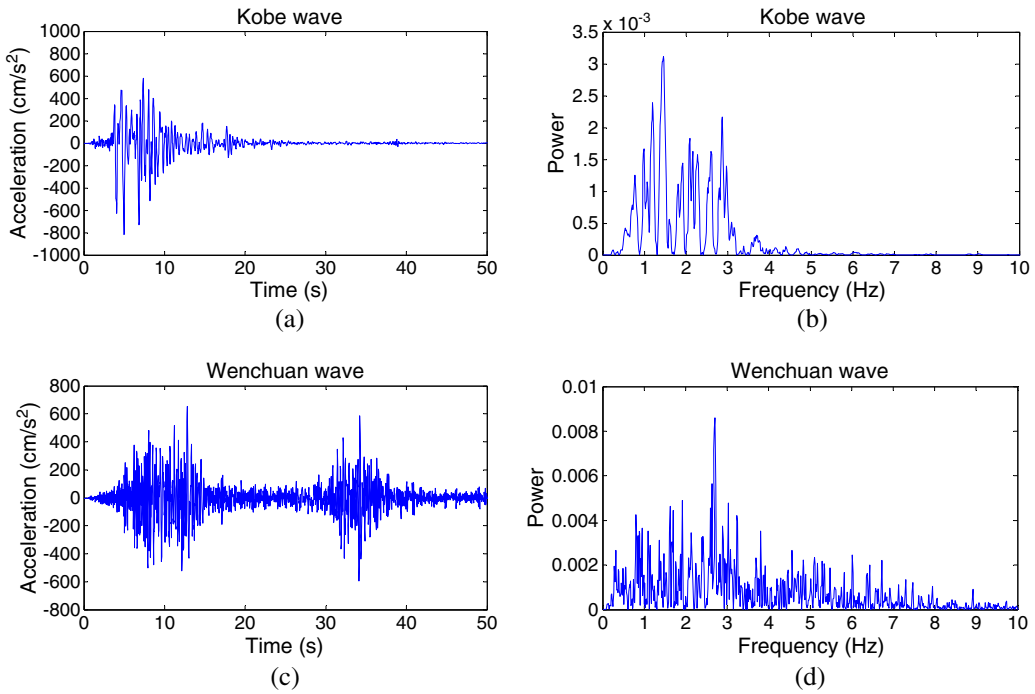

Figure 3. (a, c) Acceleration time history curves of Kobe wave and Wenchuan wave; (b, d) corresponding fast Fourier transforms of Kobe wave and Wenchuan wave.

DOI: 10.1002/eqe

the base motion were monitored with accelerometers and direct displacement gauges. All the test data were collected by a computer-controlled system and were transferred to a personal computer for further analysis.

3. SYSTEM RESPONSE

The maximum displacement responses at the roof of the test frame (X_3) and their root mean square (r.m.s.) value (σ_3) are shown in Table I for all the test runs (the response of the uncontrolled frame under SHW2 (0.2 g) wave was so large that it may cause the frame to collapse; consequently, this test was not carried out in the experiment). The r.m.s of displacement is an index of the vibration energy. It can be seen that: (i) the frame with multi-unit particle dampers has a smaller response of displacement compared with that of the frame without particle dampers; (ii) The vibration reduction effect (reduction effect = (response of system without dampers – response of system with dampers) / response of system without dampers) of the r.m.s of displacement is much better than that of the peak displacement, in which the former is 11.7–40.4%, and the latter is 4.4–18.6%. This means multi-unit particle dampers can help the primary system to dissipate a lot of input earthquake energy. Additionally, the displacement can also be effectively reduced. (iii) The vibration reduction effect is different under different seismic inputs. In the experiment, the system under Wenchuan excitation resulted in the worst reduction effect. The reason may lie in the frequency characterization of the input earthquake excitations. Figure 3 shows the excitation of Kobe wave and Wenchuan wave in the time domain and frequency domain, respectively. One can see that the main frequency of Kobe wave is around 1.4 Hz, which is near the fundamental frequency of the primary system (1.07 Hz), whereas that of Wenchuan wave is around 2.7 Hz. Another reason may be that the displacement response of the frame under Wenchuan wave is smaller than that under other inputs, which leads to milder movements for particles in the container. There are fewer collisions between the particles and the primary system and the particle dampers dissipate less input energy. Consequently, the system generated the worst reduction effect under Wenchuan wave.

Not only can the displacement be reduced, the acceleration and interstory drift can also be attenuated in most cases. Table II shows the maximum acceleration responses at the roof (A_3) and the maximum interstory responses at the first floor (X_1) of the test frame. One can see that the acceleration and interstory drift of the controlled frame are smaller than that of the uncontrolled frame in most cases (except for the Wenchuan wave (0.2 g) case); however, the reduction effect of interstory drift (0.1–6.4%) is not as good as that of acceleration (2.3–19.1%). The reason may lie on the position of the damper, which is on the top floor of the frame. From Table II, the response reduction effects of the frame with particle dampers under Wenchuan wave are also the worst, especially for the top

Table I. Maximum displacement and their r.m.s. value (mm) at the roof of the test frame.

Seismic input	Peak input value (g)	Test frame with dampers		Test frame without dampers		Reduction effect (%)	
		X_3	σ_3	X_3	σ_3	X_3	σ_3
Kobe	0.05	38.335	7.385	42.727	12.401	10.3	40.4
	0.1	66.665	12.899	73.984	19.882	9.9	35.1
	0.2	110.979	17.356	116.063	21.807	4.4	20.4
El Centro	0.05	30.366	6.552	33.131	10.525	8.3	37.7
	0.1	49.319	11.044	53.936	18.095	8.6	39.0
	0.2	81.416	15.308	92.143	24.672	11.6	38.0
Wen chuan	0.05	23.118	5.915	26.073	6.699	11.3	11.7
	0.1	43.994	10.991	47.435	12.470	7.3	11.9
	0.2	75.354	18.063	78.938	20.889	4.5	13.5
SHW2	0.05	70.774	18.337	83.027	29.306	14.8	37.4
	0.1	96.420	23.228	118.393	29.656	18.6	21.7
	0.2	—	—	—	—	—	—

DOI: 10.1002/eqe

Table II. Maximum acceleration at the roof (g) and maximum interstory drift at the first floor (mm) of the test frame.

Seismic input	Peak input value (g)	Test frame with dampers		Test frame without dampers		Reduction effect (%)	
		A_3 (g)	X_1 (mm)	A_3 (g)	X_1 (mm)	A_3	X_1
Kobe	0.05	0.213	19.185	0.240	20.498	11.3	6.4
	0.1	0.366	33.713	0.398	33.749	8.0	0.1
	0.2	0.591	58.178	0.637	59.025	7.2	1.4
El Centro	0.05	0.178	18.080	0.198	18.419	10.1	1.8
	0.1	0.296	29.627	0.311	30.703	4.8	3.5
	0.2	0.501	52.471	0.567	55.743	11.6	5.9
Wen chuan	0.05	0.168	14.335	0.172	14.757	2.3	2.9
	0.1	0.318	26.947	0.345	28.479	7.8	5.4
	0.2	0.474	60.269	0.452	60.833	−4.9	0.9
SHW2	0.05	0.362	35.587	0.430	37.155	15.8	4.2
	0.1	0.473	58.534	0.586	60.075	19.1	2.6
	0.2	—	—	—	—	—	—

floor's acceleration in the 0.2 g case, which is enlarged. This is also an evidence of the complex influence of input excitations.

The time histories of the responses of the test frame with multi-unit particle dampers are also much smaller than those of the uncontrolled frame. Figure 4 shows the displacement time history at the roof level of the test frame, in which a solid line represents the response of the frame with a particle damper, and the dot line shows the response of the uncontrolled frame. From Figure 4, one can see that the particle damper system not only reduces the maximum response of the displacement, but also makes the whole time history attenuate quickly, so that the response most of the time is reduced. This is also an additional evidence that the r.m.s. of the displacement reduction effect is better than the maximum displacement reduction effect. Another interesting phenomenon in Figure 4 is that the responses of the controlled and uncontrolled systems are the same at the very beginning of the time

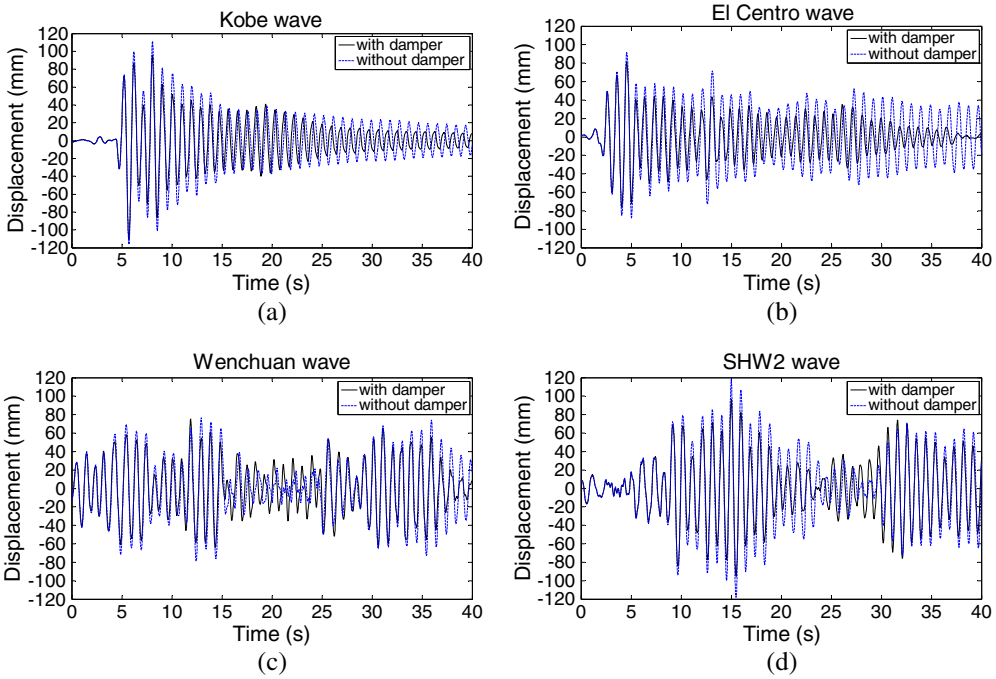

Figure 4. Displacement time history at roof level of the test frame. (a) Kobe wave (0.2 g); (b) El Centro wave (0.2 g); (c) Wenchuan wave (0.2 g); and (d) SHW2 wave (0.1 g).

DOI: 10.1002/eqe

period; after a while, the controlled curve begins to decay quickly. This is a similar phenomenon encountered in the operation of a tuned mass damper. The vibration reduction effect is not good at the very beginning and becomes better as time goes by. The reason is that it takes some time for particles in the container to impact the wall of the container. After certain impacts, the particle damper system starts to dissipate the input energy by momentum transfer.

Figure 5 shows the maximum displacement and maximum acceleration at every floor of the test frame under different seismic inputs. One can find that generally, each floor of the frame can achieve vibration attenuation in almost all test inputs, although the reduction effects have slight differences. Another interesting observation in Figure 5(c) is that the maximum acceleration of the first floor is larger than that of the roof under Wenchuan wave (0.2 g). The reason is that a structure is like a filter, which can remove the high frequency component of the excitation when the earthquake wave is transmitting from the ground to the upper structure, and finally the fundamental frequency dominates the vibration of the structure. However, in the lower floor of the structure, there may still be a lot of high frequency components. On the other hand, the acceleration is related to the square of the frequency. Consequently, for the first floor, there may exist a situation when, although the displacement is small, the maximum acceleration is larger than the top floor.

Figure 6 gives a series of snapshots from a shot video to show a typical time period of the motion of the system with particles. It can be found that in a certain period, plug flow motions of the particles, rather than unordered movements, can be observed. The particles in the container are excited along the X direction only; however, as there are collisions (including oblique impacts) between particles and between particle and the container, some particles may also move in the Y direction, which lead to unordered movements. The plug flow phenomenon is a similar qualitative behavior to what occurs in a single-particle impact damper when operating with two impacts per cycle [22]. In plug flow mode, the particles tend to move together and make fewer collisions between them. This pattern of movements can achieve better vibration reduction for the primary system. However, this does not mean a single-particle impact damper is more appropriate in real applications because there are no collisions between particles. The reasons are: (i) there may be larger noise for a single-particle impact damper during the impact; (ii) there is a very significant level in reduction in the impulsive force transmitted by a single-particle damper to the primary system in comparison with an equivalent collection of particles operating in slug mode; and (iii) it is more sensitive to the changes of the system parameters, compared with multi-unit particle dampers. For example, for

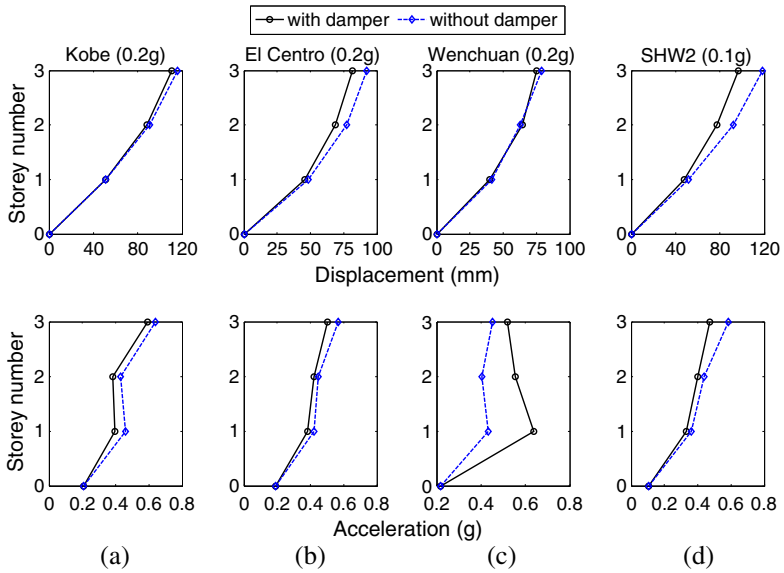

Figure 5. Maximum displacement (the upper line) and maximum acceleration (the lower line) at every floor of the test frame. The circle shows the response of the test frame without damper, while the diamond shows the response with damper. (a) Kobe wave (0.2 g); (b) El Centro wave (0.2 g); (c) Wenchuan wave (0.2 g); and (d) SHW2 wave (0.1 g).

DOI: 10.1002/eqe

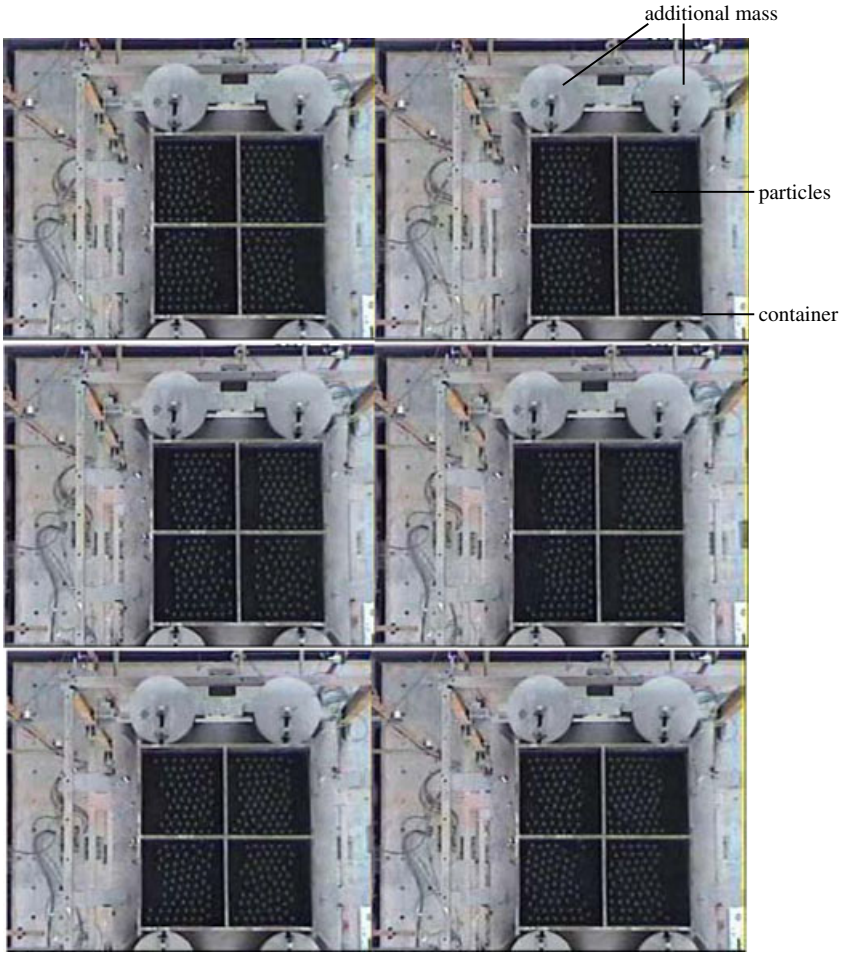

Figure 6. Snapshots of the motion of the test frame with multi-unit particle dampers under El Centro (0.2 *g*) input.

multi-unit particle dampers, the vibration attenuation to changes in container length (dx) decreases, which results in a wider optimum margin of dx for the multi-unit particle damper [23]. Hence, the multi-unit particle damper is more robust and may be more appropriate in engineering practices. On the other hand, both the experimental [11] and numerical studies [24] show that the plug flow mode usually corresponds to optimum vibration attenuation effects for particle dampers.

From the shaking table test results mentioned above, it is shown that by using properly designed multi-unit particle dampers, a lightly damped MDOF primary system can achieve a reasonable reduction in its response with a small weight penalty (2.25%). The vibration attenuation of the r.m.s. of displacement is much better than that of the maximum displacement or maximum acceleration.

4. ANALYTICAL / COMPUTATIONAL SOLUTION

4.1. Analytical method

Figure 2(a) in Section 2 shows the model of a three-storey frame with multi-unit particle dampers. The equation of motion of the primary system can be written as

$$\mathbf{M}\ddot{\mathbf{X}} + \mathbf{C}\dot{\mathbf{X}} + \mathbf{K}\mathbf{X} = \mathbf{F} + \mathbf{E}\ddot{x}_{\mathbf{g}} \tag{1}$$

$$\mathbf{M} = \mathrm{diag}[M_1 \quad M_2 \quad \ldots \quad M_{\mathrm{N}}] \tag{2}$$

DOI: 10.1002/eqe

$$\mathbf{C} = \begin{bmatrix} C_1 + C_2 & -C_2 & & & \\ -C_2 & (C_2 + C_3) & -C_3 & & \\ & & & \ddots & -C_N \\ & & & -C_N & C_N \end{bmatrix} \tag{3}$$

$$\mathbf{K} = \begin{bmatrix} K_1 + K_2 & -K_2 & & & \\ -K_2 & (K_2 + K_3) & -K_3 & & \\ & & & \ddots & -K_N \\ & & & -K_N & K_N \end{bmatrix} \tag{4}$$

$$\mathbf{X} = [\, X_1 \quad X_2 \quad \ldots \quad X_N \,]^T \tag{5}$$

$$\mathbf{F} = [\, 0 \quad 0 \quad \ldots \quad F_N \,]^T \tag{6}$$

$$\mathbf{E} = [\, -M_1 \quad -M \quad \ldots \quad -M_N \,]^T, \tag{7}$$

where **M**, **C**, **K** are mass, damping and stiffness matrices, respectively; **F**, **E** and $\ddot{x}_g$ are the contact force vector, matrix-induced ground acceleration, and ground acceleration, respectively. X_i is the relative displacement of the i-th floor with respect to the ground; $M_{,i}$ $C_{,i}$ K_i are the mass, damping and stiffness of the i-th floor, respectively; and F_i is the contact force acting on the i-th floor by particles ($i = 1, 2, \ldots, N$), which is the linkage between particles and the primary system.

Although the response of the multi-unit particle damper system can be analyzed using Equation (1), it requires considerable computational effort; consequently, the assumption that the behaviors of the particles in each container are the same is used to estimate the performance of the system. The contact force of the primary system with all particles can be considered to be equal to the product of the number of containers and the contact force of the primary system with the particles in one container. Therefore, the particle number that should be considered in the numerical simulation can be reduced to the particle number in one container. This convenience makes it possible to considerably reduce the calculation time. On the other hand, if the containers have dissimilar dimensions, then a more robust performance may be obtained.

The DEM is a numerical scheme that allows finite rotations and displacements of discrete bodies that are interacting according to local contact laws, and are described by Newton's equation of motion. It is based on the idea that the time step chosen may be so small that, during a single time step, disturbances cannot propagate from any particle further than its immediate neighbors. Then, at all times, the forces acting on any particle are determined exclusively by its interaction with the particles with which it is in contact. This method is applied in this study to capture the behavior of the entire system in detail. With this technique, the position and contact force of the individual particle and the primary system can be traced at every single time step. Consequently, the governing equation for a particle i can be written as

$$m_i \ddot{\mathbf{p}}_\mathbf{i} = m_i \mathbf{g} + \sum_{j=1}^{k_i} \left(\mathbf{F}_{ij}^n + \mathbf{F}_{ij}^t \right) \tag{8}$$

$$\mathbf{I}_i \ddot{\mathbf{\Phi}}_\mathbf{i} = \sum_{j=1}^{k_i} \mathbf{T}_{ij}, \tag{9}$$

where m_i is the mass of particle i, $\mathbf{I}_\mathrm{i}$ is the moment of inertia of particle i and **g** is the acceleration vector due to gravity, $\mathbf{p}_\mathrm{i}$ is the position vector of the center of gravity of particle i, $\mathbf{\Phi}_i$ is the angular

DOI: 10.1002/eqe

displacement vector, $\mathbf{F}_{ij}^{n}$ is the normal contact force between particle i and particle j (if particle i is in contact with container wall, then j denotes that wall), and $\mathbf{F}_{ij}^{t}$ is the tangential contact force. The contact forces act at the contact point between particle i and particle j rather than the particle center, and they will generate a torque, $\mathbf{T}_{ij}$, causing particle i to rotate. For a spherical particle of radius r_i, $\mathbf{T}_{ij}$ is given by $\mathbf{T}_{ij} = r_i \mathbf{n}_{ij} \times \mathbf{F}_{ij}^{t}$, where $\mathbf{n}_{ij}$ is the unit vector from the center of particle i to the center of particle j and $\times$ denotes the cross product. These interparticle forces are summed over the k_i particles in contact with particle i.

A number of contact models can be used to quantify the normal and tangential contact forces; however, this is still an active research topic, particularly for the tangential forces [26–28]. The present simulation study uses a linear contact model in the normal direction and Coulomb's law of friction in the tangential direction.

Figure 7 presents the linear contact model between the particle and the wall in the normal direction, where a stiff spring and a viscous dashpot are acted in parallel to simulate the contact force. Parameters k_2 and c_2 are the stiffness and the damping constant of the impact damper 'stops', respectively ('stops' are used here to name the combined mechanics of the spring and the dashpot between the particle and the wall [29]). The variable $\omega_2 = \sqrt{k_2/m}$ is the natural frequency, which can be used to simulate a rigid barrier to any degree of accuracy, by a proper choice. On the basis of previous studies [22], the ratio of $\omega_2/\omega_n \geqslant 20$ is appropriate to represent a 'stiff' barrier (ω_n is the fundamental frequency of the primary system). The parameter $\zeta_2 = c_2/2m\omega_2$ is the damping ratio, which can be used to simulate inelastic impacts, ranging from the completely plastic up to the elastic one, so that the value of any desired coefficient of restitution e can be adjusted by selecting the proper value for ζ_2. Similarly, k_3, ω_3, c_3 and ζ_3 are the stiffness, natural frequency of the spring, and the damping coefficient and damping ratio of the damper, respectively, in the interparticle contact model along the normal direction. Hence, the normal contact force is expressed by

$$F_{ij}^{n} = \begin{cases} k_2\delta_n + 2\zeta_2\sqrt{mk_2}\dot{\delta}_n & \delta_n = r_i - \Delta_i \quad \text{(particle} - \text{wall)} \\ k_3\delta_n + 2\zeta_3\sqrt{\dfrac{m_i m_j}{m_i + m_j}k_3} \quad \dot{\delta}_n & \delta_n = r_i + r_j - \left|\mathbf{p}_j - \mathbf{p}_i\right| \quad \text{(particle} - \text{particle)} \end{cases}, \tag{10}$$

where δ_n and $\dot{\delta}_n$ are the displacement and velocity of particle i relative to particle j, respectively, and Δ_i is the distance from the center of particle i to the wall.

Considering Coulomb's law of friction, the tangential contact force is expressed by

$$F_{ij}^{t} = -\mu_s F_{ij}^{n} \dot{\delta}_t / \left|\dot{\delta}_t\right|, \tag{11}$$

where μ_s is the coefficient of friction between any two particles or between a particle and the wall of the container and $\dot{\delta}_t$ is the velocity of particle i relative to particle j or the wall in the tangential direction.

The time step should be small enough to capture the collision details in particle damper simulation and it is also important in DEM computation. When the time step is about one-fifth the duration of the contact, it is usually sufficient to ensure the impacts are not missed and to ensure numerical stability [30]. In typical DEM computations, the time step is usually chosen to be a fraction of the critical

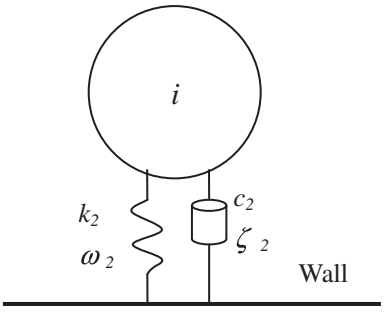

Figure 7. Normal contact force model between a particle and the wall.

DOI: 10.1002/eqe

time step. The critical time step is computed using [31]

$$\Delta t_c = \frac{2}{\omega_{\max}}\left(\sqrt{1+\zeta^2}-\zeta\right) \approx \alpha \frac{2}{\sqrt{\frac{k_{\max}}{m_{\min}}}}\left(\sqrt{1+\zeta^2}-\zeta\right), \tag{12}$$

where $k_{\max}$ is the largest interelement spring stiffness, $m_{\min}$ is the mass of the smallest element, hence $\sqrt{k_{\max}/m_{\min}}$ is a crude estimate of the highest natural frequency of vibration for the model. The factor α is a user-selected parameter. Computational experience shows that values of α near 0.1 are typically satisfactory to provide a stable computation [32].

With the above in mind, the procedure for calculating the response of the particle dampers used in this study can now be illustrated. First, consider the relative position of the particles and walls. If $\delta_n > 0$, the contact force acting on the particle can be determined from Equations (10) and (11), whereas if $\delta_n \le 0$, no contact force is produced. Second, sum all the contact forces acting on this particle, including interparticle forces and particle–wall forces, if they exist. Third, the particle motion can be analyzed by Equations (8) and (9). The same procedure is repeated for all the particles. Finally, the components of the contact force **F** acting on the primary system are given by the summation of all the contact forces between the particles and the wall of the container, respectively. By using the components of the contact force **F**, the equation of motion for the primary system, Equation (1) is updated.

As part of the study reported herein, a code was programmed according to the above-mentioned procedure, and the fourth-order Runge–Kutta method was applied to solve the resulting system of nonlinear ordinary differential equations [33,34].

4.2. *Computational results*

The parameters used in the computational simulation are listed in Table III. The calculated time step is 1×10^{-4} s, and meets all the requirements mentioned in the above section.

$$\mathbf{M} = \begin{bmatrix} 1915 & 0 & 0 \\ 0 & 1915 & 0 \\ 0 & 0 & 2124 \end{bmatrix} \text{kg} \quad \mathbf{K} = \begin{bmatrix} 933000 & -466500 & 0 \\ -466500 & 933000 & -466500 \\ 0 & -466500 & 466500 \end{bmatrix} \text{N/m} \quad \zeta_1 = 0.013$$

Figures 8 and 9 show the calculated and experimental displacement and acceleration time histories at roof level of the test frame with multi-unit particle dampers under $0.2\,g$ earthquake excitations, respectively. It is shown that the calculated response time history curves have good agreements with the experimental ones during most time periods, in which the displacement curves fit better than the acceleration curves. This is because the displacement is the integration of the acceleration and the curve is smoother. As to the acceleration response, there is an impulse and a sudden change at the instant that particles impact the container.

Table IV illustrates the comparison of simulation results and experimental results for the maximum displacement of the roof of the test frame with the particle damper system. It can be seen from

Table III. Values of system parameters.

Parameter	Value
Container number	4
Total particle number	63×4 ($\mu = 2.25\%$)
Diameter of the particle (mm)	50.4
Density of the particle (kg/m^3)	7800
Coefficient of friction	0.5
Critical damping ratio of the damper	0.1
Stiffness of the spring between particle and wall (N/m)	100000
Stiffness of the spring between particle and particle (N/m)	100000
Time step (second)	1×10^{-4}

DOI: 10.1002/eqe

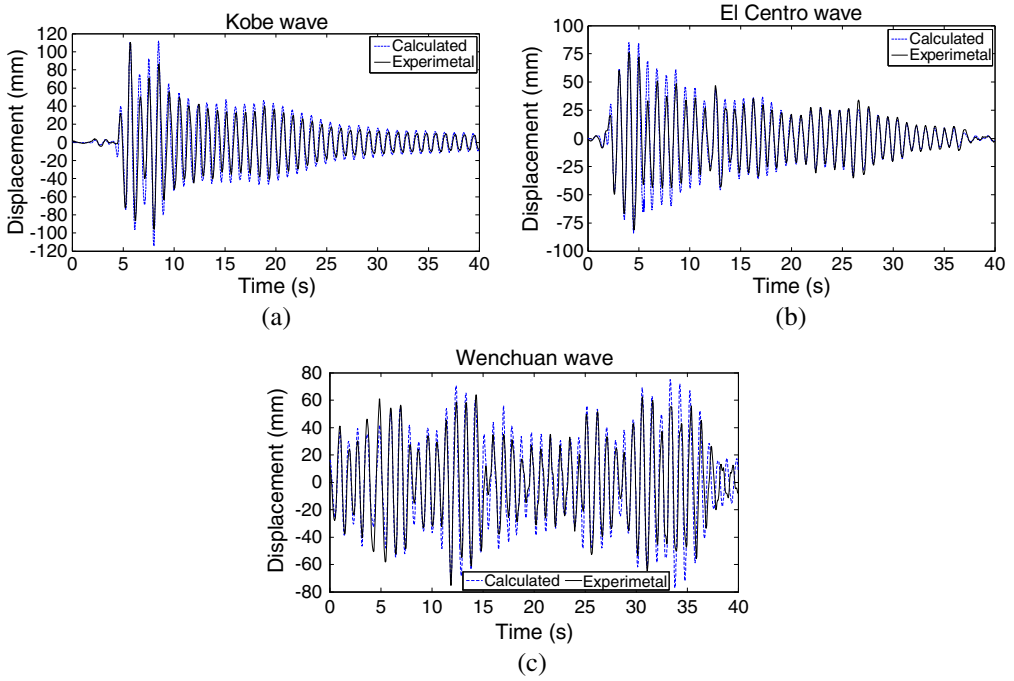

Figure 8. Displacement time histories at roof level of the test frame with multi-unit particle dampers under 0.2 *g* earthquake excitations. (a) Kobe wave; (b) El Centro wave; and (c) Wenchuan wave.

Figures 8 and 9 and Table IV that there is a good agreement between the test and analysis results, which demonstrates that the proposed analytical method can yield estimates of the response of the particle damper system under earthquake excitations with an acceptable accuracy.

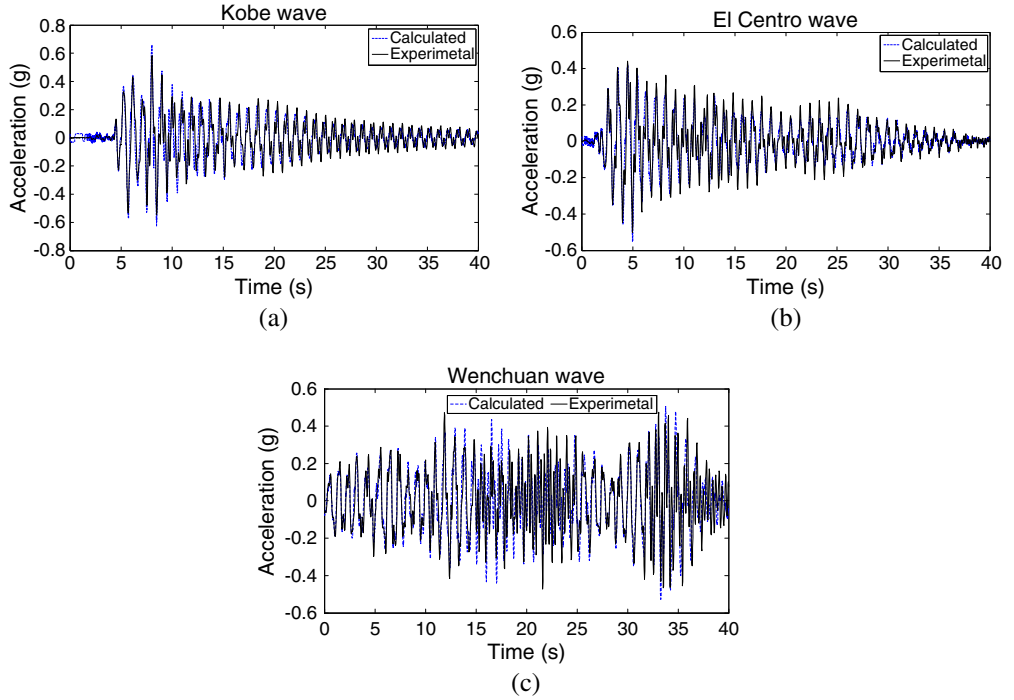

Figure 9. Acceleration time histories at roof level of the test frame with multi-unit particle dampers under 0.2 *g* earthquake excitations. (a) Kobe wave; (b) El Centro wave; and (c) Wenchuan wave.

DOI: 10.1002/eqe

Table IV. Comparison of calculated results and experimental results for the maximum displacement of the roof of the test frame with multi-unit particle dampers.

Seismic input	Peak input value (g)	Calculated value (mm)	Experimental value (mm)	Error (%)
Kobe	0.05	37.726	38.335	−1.6
	0.1	67.638	66.665	1.5
	0.2	114.519	110.979	3.2
El Centro	0.05	29.713	30.366	−2.2
	0.1	49.472	49.319	0.3
	0.2	84.206	81.416	3.4
Wenchuan	0.05	22.418	23.118	−3.0
	0.1	42.113	43.994	−4.3
	0.2	77.174	75.354	2.4
SHW2	0.05	69.821	70.774	−1.3
	0.1	98.465	96.420	2.1
	0.2	—	—	—

5. CONCLUSIONS

Although many researchers [6–8,11–13,18] have presented the results of many experiments on particle dampers (including single-unit impact damper) with an SDOF primary system under harmonic or random excitations, the performance of such nonlinear devices is a highly complex nonlinear process involving energy dissipation and momentum exchange, and is not amenable to exact analytical solutions. Consequently, there are no guidelines currently existing for determining the optimum strategies for maximizing the performance of particle dampers under dynamic loads.

This paper further investigated the performance of multi-unit particle dampers used for controlling the vibrations of structures under earthquake inputs. It was found that a multi-unit particle damper system has good performance in reducing the seismic response of structures, for example, acceleration, displacement, r.m.s. of displacement, and interstory drift, in which the r.m.s. response reduction effect is the best. The response of the test frame under all the seismic inputs used in this study was reasonably reduced, although the degree of the vibration reduction effect was quite variable. From the shaking table test, it was also shown that the excitation characterization influences the performance of the particle damper system, and the particle movements of plug flow pattern can yield good vibration attenuation effects.

Using well-established discrete particle modeling approaches, all significant interaction forces among the particles and with the rigid walls of their container were properly accounted for, including sliding friction, gravitational forces, and oblique impacts. This analytical/computational method was verified by shaking table test results, and could yield reasonably accurate estimates of the response of the MDOF system with multi-unit particle dampers.

Because of the high nonlinearity of the particle damper system, a lot of parameters can influence its behavior, for example, frequency spectrum characterization of the excitation and its intensity, the mass ratio of particles, and their moving patterns. From the experimental and analytical results, it was found that by using properly designed multi-unit particle dampers, a lightly damped MDOF primary system can achieve a reasonable reduction in its response with a small weight penalty, provided that the container dimensions allow particle movement in a plug-flow pattern, without gathering in many layers.

ACKNOWLEDGEMENT

Financial support from the National Natural Science Foundation of China through grant 51108346, 90815029 and 51021140006 are highly appreciated. The work is also supported by Kwang-Hua Fund for College of Civil Engineering, Tongji University.

REFERENCES

1. Spencer BF, Dyke SJ, Deoskar HS. Benchmark problems in structural control: part I—Active Mass Driver system. *Earthquake Engineering and Structural Dynamics* 1998; **27**(11):1127–1139.

DOI: 10.1002/eqe

2. Leung AYT, *et al*. Particle swarm optimization of TMD by non-stationary base excitation during earthquake. *Earthquake Engineering and Structural Dynamics* 2008; **37**(9):1223–1246.
3. Niwa N, et al. Dynamic loading test and simulation analysis of full-scale semi-active hydraulic damper for structural control. *Earthquake Engineering and Structural Dynamics* 2000; **29**(6):789–812.
4. Naeim F, Lew M, Carpenter LD, Youssef NF, Rojas F, Saragoni GR, Adaros MS. Performance of tall buildings in Santiago, Chile during the 27 February 2010 offshore Maule, Chile earthquake. *The Structural Design of Tall and Special Buildings* 2011; **20**(1):1–16.
5. Masri SF, Caughey TK. On the stability of the impact damper. *Journal of Applied Mechanics* 1966; **33**:586–592.
6. Saeki M. Analytical study of multi-particle damping. *Journal of Sound and Vibration* 2005; **281**(3–5):1133–1144.
7. Thomas MD, Knight WA, Sedek MM. The impact damper as a method of improving cantilever boring bars. *Journal of Engineering Industry, ASME* 1975; **97**(3):859–866.
8. Ema S, Marui E. Fundamental study on impact dampers. *International Journal of Machine Tools and Manufacture* 1994; **34**(3):407–421.
9. Yang MY, et al. Development of a design curve for particle impact dampers. *Noise Control Engineering Journal* 2005; **53**(1):5–13.
10. Li KN, Darby AP. Experiments on the effect of an impact damper on a multiple-degree-of-freedom system. *Journal of Vibration and Control* 2006; **12**(5):445–464.
11. Papalou A, Masri SF. Performance of particle dampers under random excitation. *Journal of Vibration and Acoustics-Transactions of the Asme* 1996; **118**(4):614–621.
12. Papalou A, Masri SF. An experimental investigation of particle dampers under harmonic excitation. *Journal of Vibration and Control* 1998; **4**(4):361–379.
13. Papalou A, Masri SF. Response of impact dampers with granular materials under random excitation. *Earthquake Engineering and Structural Dynamics* 1996; **25**(3):253–267.
14. Liu W, Tomlinson GR, Rongong JA. The dynamic characterisation of disk geometry particle dampers. *Journal of Sound and Vibration* 2005; **280**(3–5):849–861.
15. Xu ZW, Chan KW, Liao WH. An empirical method for particle damping design. *Shock and Vibration* 2004; **11**:647–664.
16. Fang X, Tang J. Granular Damping in Forced Vibration: Qualitative and Quantitative Analyses. *Journal of Vibration and Acoustics* 2006; **128**(4):489–500.
17. Wu CJ, Liao WH, Wang MY. Modeling of granular particle damping using multiphase flow theory of gas-particle. *Journal of Vibration and Acoustics* 2004; **126**(2):196–201.
18. Saeki M. Impact damping with granular materials in a horizontally vibrating system. *Journal of Sound and Vibration* 2002; **251**(1):153–161.
19. Mao KM, Wang MY, Xu ZW, Chen TN. DEM simulation of particle damping. *Powder Technology* 2004; **142**(2–3):154–165.
20. Hu L, Huang Q, Liu Z. A non-obstructive particle damping model of DEM. *International Journal of Mechanics and Materials in Design* 2008; **4**(1):45–51.
21. Wong CX, Daniel MC, Rongong JA. Energy dissipation prediction of particle dampers. *Journal of Sound and Vibration* 2009; **319**(1–2):91–118.
22. Masri SF. Steady-State Response of a Multidegree System with an Impact Damper. *Journal of Applied Mechanics-Transactions of the Asme* 1973; **40**(1):127–132.
23. Nayeri RD, Masri SF, Caffrey JP. Studies of the performance of multi-unit impact dampers under stochastic excitation. *Journal of Vibration and Acoustics* 2007; **129**(2):239–251.
24. Lu Z, Masri SF, Lu XL. Studies of the performance of particle dampers attached to a two-degree-of-freedom system under random excitation. *Journal of Vibration and Control* 2010; doi:10.1177/1077546310370687.
25. Cundall PA, Strack O. A distinct element model for granular assemblies. *Geotechnique* 1979; **29**:47–65.
26. Du YC, Wang SL. Energy dissipation in normal elastoplastic impact between two spheres. *Journal of Applied Mechanics* 2009; **76**(6):061010–061017.
27. Elperin T, Golshtein E. Comparison of different models for tangential forces using the particle dynamics method. *Physica A: Statistical and Theoretical Physics* 1997; **242**(3–4):332–340.
28. Di Renzo A, Di Maio FP. Comparison of contact-force models for the simulation of collisions in DEM-based granular flow codes. *Chemical Engineering Science* 2004; **59**(3):525–541.
29. Masri SF, Ibrahim AM. Response of Impact Damper to Stationary Random Excitation. *Journal of the Acoustical Society of America* 1973; **53**(1):200–211.
30. Ghaboussi J, Barbosa R. Three-dimentional discrete element method for granular materials. *International Journal for Numerical and Analytical Methods in Geomechanics* 1990; **14**:451–472.
31. Tavarez FA. Discrete element method for modeling solid and particulate materials. *Engineering Mechanics*. University of Wisconsin-Madison: Madison, 2005.
32. Jensen RP, Bosscher PJ, Plesha ME, DEM simulation of granular media-structure interface: effects of surface roughness and particle shape. *International Journal for Numerical Methods in Geomechanics* 1999; **23**:531–547.
33. Lu Z, Lu XL, Masri SF. Studies of the performance of particle dampers under dynamic loads. *Journal of Sound and Vibration* 2010; **329**(26):5415–5433.
34. Lu Z, Masri SF, Lu XL. Parametric studies of the performance of particle dampers under harmonic excitation. *Sturctural Control and Health Monitoring* 2011; **18**(1):79–98.

DOI: 10.1002/eqe